Spectroscopy and Dynamics of Excited Harpooning Reactions: The Photodepletion Action Spectrum of the Ba···FCH_3 Complex

S. Skowronek, R. Pereira, and A. González Ureña*

Unidad de Laseres y Haces Moleculares, Instituto Pluridisciplinar, Universidad Complutense de Madrid, Juan XXIII, 1, 28040 Madrid, Spain

Received: January 31, 1997; In Final Form: April 11, 1997[⊗]

A laser time-of-flight mass spectrometer setup used to investigate the spectroscopy and dynamics of weakly bound complexes is described. Complexes were produced by laser vaporization of metals into a supersonic expansion of helium and a solvent. The first results consisting of laser ionization and photodepletion spectra of Ba···$(FCH_3)_n$ for $1 \leq n \leq 3$ are reported. The measurement of the Ba···FCH_3^+ signal as a function of the ionization photon energy allowed estimation of the complex ionization potential, which was found to be 4.5 ± 0.1 eV. The photodepletion spectrum of the Ba···FCH_3 complex displayed two distinct regions. At longer wavelengths it showed a high cross-section (60−70 Å^2) and a well-defined vibrational structure, while a much smaller cross-section (2−4 Å^2), with a more diffuse structure, appeared at shorter wavelengths. In addition, clear resonances were observed at longer wavelengths, indicating a significant coupling between the bound excited potential of the complex and the (open channel) ionic potential leading to $BaF^* + CH_3$ reaction products. All of these features are discussed, taking into account the interplay between the spectroscopy and dynamics associated with each electronically excited state of the complex that governs the photoinitiated harpooning reaction.

I. Introduction

In order to construct the potential energy surface of a chemical reaction, a detailed understanding of the processes involved in the reaction is needed. The disappearance of reactants and appearance of products, i.e., the before and after of the reaction, are events that are precisely determined with the current laser and molecular beam techniques.[1] However, to have a comprehensive description of the reaction, it is indispensable to know the properties of the intermediate species between reactives and products, namely, the transition state region,[2] whose investigation constitutes one of the most active research fields nowadays. Several approaches have been developed to access this part of the potential energy surface.[2−13]

Zewail's group has probed the transition states of reactions in real time using femtosecond lasers.[3,4] Soep's group[7,10−13] pioneered the method of condensing the reagents in a van der Waals or weakly bound complex and measured the action spectra for the reactions of metals such as Hg[10] and Ca[11−13] with H_2 and hydrogen halides. They monitored the yield of electronically excited product using laser induced fluorescence as the probing technique. Polanyi's group[14,15] used the van der Waals approach to study the reaction dynamics of the complexes of Na with CH_3Cl, CH_3F, and PhF. They produced the species in crossed-beam experiments and measured the photodepletion of the complexes through time-of-flight mass spectrometry (TOFMS).

In the present work TOFMS was used to investigate the photodepletion spectrum of the Ba···FCH_3 complex. Although the main goal of our study has motivations similar to many of the studies mentioned above and particularly follows that of Polanyi's group,[14,15] there are clear differences between them. First of all, we have used barium metal, e.g., a two electron atom, which may result in a different dynamical picture even considering the same electron transfer mechanism between the atom and the solvent molecule. From the experimental point of view, as in Soep's experiments,[10−13] the weakly bound complexes were produced in a supersonic expansion of a mixture of helium, a solvent (CH_3F), and the laser desorbed metal (barium). However, we have used the TOFMS method of detection rather than the specific chemiluminescence action spectra adopted by Soep's group[10−13] for the Ca···HX (X = Cl, Br) complexes.

It is clear that the TOFMS method used here is complementary to laser-induced chemiluminescence studies applied in other related systems. Thus, to undertake such an approach is useful not only because it provides additional information but also because sometimes it can be the only possible method of products characterization as, for example, in dark channel reactions. Another motivation is based on the series of studies of bimolecular reactions, carried out in our laboratory, with excited alkaline-earth atoms in crossed-beam techniques (full collisions).[6] It would certainly be very interesting to compare the information obtained in those experiments with that obtained from the present "half-collision" studies and to draw a global picture about the dynamics and stereodynamics of these excited electron transfer reactions.

In this paper we present the photodepletion action spectrum of the Ba···FCH_3 complex in the range 547−630 nm. Two different excited electronic states of the complex have been observed. They may well correlate with the two different alignments of the barium p orbital with respect to the interparticle distance, the complex interaction axis, considering the CH_3F reagent as a closed-shell particle. We can anticipate that these two electronically excited states show not only a specific spectroscopy but also a distinct dynamics as a result of a different coupling to the ionic potential leading to the reaction products. The results are discussed in light of the spectroscopy and dynamics underlying the complex photofragmentation following laser excitation and the subsequent reactive and nonreactive fragmentation channels.

* To whom correspondence should be addressed.
[⊗] Abstract published in *Advance ACS Abstracts,* September 15, 1997.

S1089-5639(97)00385-X CCC: $14.00

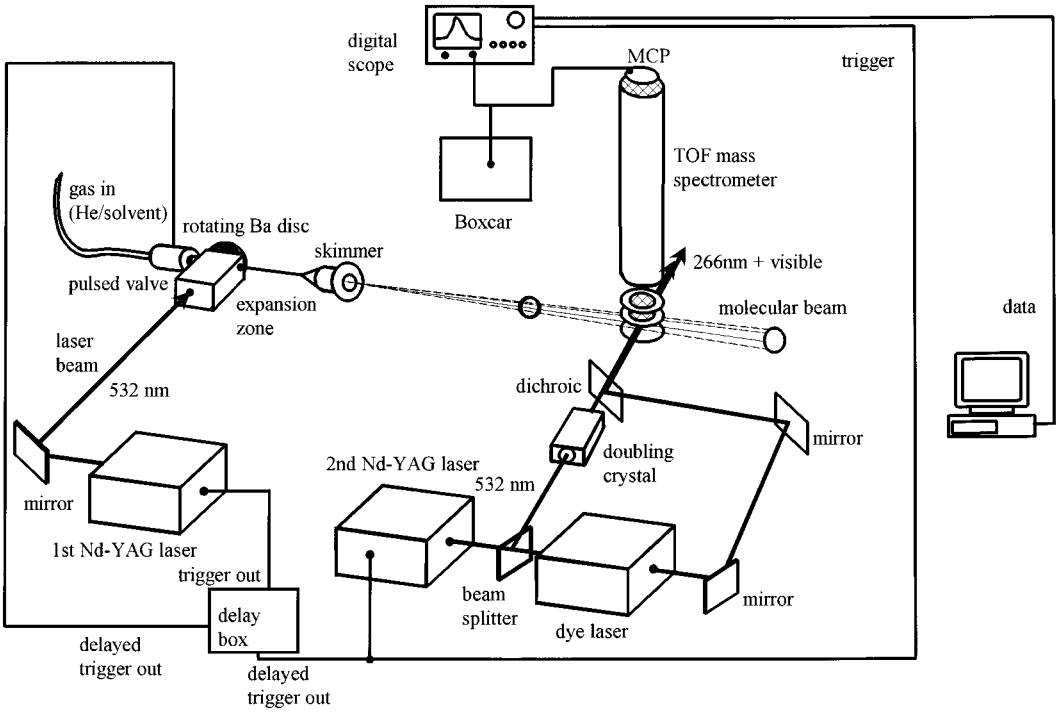

Figure 1. Experimental setup used to produce and analyze the weakly bound complexes of Ba with different solvents. The fundamental or second harmonic output of a Nd:YAG laser is focused onto the surface of a rotating barium disk. The metal vapor is injected into a mixture of helium and a solvent and expanded into a vacuum. The molecular beam is probed inside the acceleration region of a linear time-of-flight mass spectrometer.

II. Experimental Section

A schematic view of the experimental setup designed and built to produce and analyze the weakly bound complexes of barium with different solvents is shown in Figure 1. The fundamental or second harmonic output of a Nd:YAG laser (Continuum Surelite I) was focused, using a 30 cm focal length lens, onto the surface of a rotating barium disk in a classical arrangement.[16,17] The vapor of the metal was injected into a mixture of helium gas (usually 2.5 atm) and CH_3F (∼10%). The mixture was expanded supersonically through a solenoid valve (General Valve Corp.) into the first vacuum chamber. The pressure in this chamber under operating conditions was kept below 10^{-4} mbar using a Leybold diffusion pump (Leybodiff 1010, 1000 L/s) backed by a Torricelli rotary pump (RD35, 35 m^3/h).

The free expansion was skimmed (1.0 mm) before entering a second chamber containing a linear time-of-flight mass spectrometer with unit mass resolution at mass 1200 (Comstock Inc.). The pressure in the detection chamber was kept below 10^{-6} mbar at all times using two turbomolecular pumps, a Varian V300 HT (300 L/s) and a Varian V250 (250 L/s) backed by a Balzers rotary pump (DUO 016B, 16 m^3/h) and a Varian diaphragm pump (MD60, 60 L/min), respectively.

The molecular beam formed by the skimmer was interrogated in two different ways. In order to take time-of-flight mass spectra the fourth harmonic output of a Nd:YAG laser (Continuum NY80) was used to ionize the species of interest. To carry out photodepletion experiments, the second harmonic output of the same Nd:YAG laser was split into two beams. One was doubled with a thermalized KDP crystal to give 266 nm and used for ionization, and the other was used to pump a dye laser (Continuum ND60) with 0.08 cm^{-1} bandwidth. The dye laser output was used to induce the chemical reaction within the weakly bound complex. Several dyes (R575, R590, R610, R640, DCM, LDS698) and dye mixtures (R590/610, R610/640) were used to probe the spectral region of interest. The ultraviolet and dye laser beams were collinearly aligned and perpendicularly crossed with the molecular beam in the center of the acceleration region of the mass spectrometer. A diaphragm was placed at the entrance of the detection chamber to reduce the diameter of both laser beams to 4 mm. The laser energy was measured using a pyroelectric detector (Gentec). Optical synchronization was used in order to allow the dye laser to arrive earlier to the beam−laser interaction region (ca. 7−10 ns). The three events, gas pulse, desorption laser, and excitation/ionization laser, were synchronized using a homemade pulse generator.

To determine the ionization potential of the complex, UV tunable radiation was needed for ionization. In this case, the doubled output of the Nd:YAG pumped dye laser (with C500 as dye) was used.

Ions were extracted and accelerated inside the spectrometer and traveled through a 1 m field free region before they were collected by a dual microchannel plate detector (Galileo Optics). The microchannel plate output was routed to either a Tektronix TDS540 digital oscilloscope or to a boxcar integrator (Stanford Research SR250). The integration facility of the digital scope coupled to a conveniently programmed computer was also used as a boxcar integrator.

III. Energetics

Figure 2 shows an energy diagram for the Ba + $CH_3F \rightarrow$ BaF + CH_3 system. The energy of the ground state of the Ba···FCH_3 complex has been assumed to be around 0.25 eV on the basis of the existing data for analogous complexes containing alkaline-earth atoms (see ref 18 for further comments on this subject). The excited states of the complex have been estimated from the experimental information contained in the photodepletion action spectrum (see section V). Inspection of the energy diagram reveals that the ground state reaction is exoergic. Nevertheless, to the best of our knowledge, no BaF product from such a reaction has been reported in spite of a specific investigation looking for this reaction channel.[19] The absence of such a ground reaction in a full bimolecular collision is not surprising, taking into account the energy requirement for the electron transfer, presumably the mechanism responsible for the

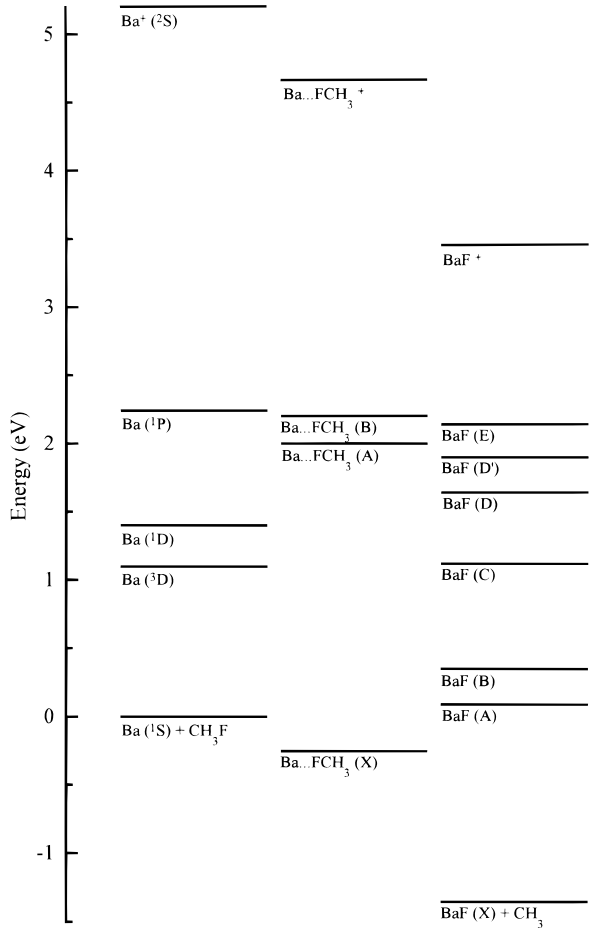

Figure 2. Energy level diagram of reactants and accessible product states. The left column shows the barium electronic energy levels and the right one the BaF energy levels. The center column displays an approximate location of the Ba···FCH_3 electronic states.

reaction, firstly, because the barium ionization potential is substantially high (i.e., 5.21 eV) and, secondly, because the energy required to access the negative ionic potential of CH_3F is even higher[20] (see also ref 21 for a review on this subject). However, BaF is present in our molecular beam, probably formed during the interaction of the vaporization laser with the metallic barium and the solvent, but that does not preclude the formation of the Ba···$(FCH_3)_n$ complexes (see below). It is also interesting to remark the many reactive as well as nonreactive channels are energetically accessible from the excited complexes. While it might represent a difficulty in interpreting the recorded data, it certainly provides a good example to be studied in detail and with enough resolution so that a deep insight can be gained of the interplay between the dynamics and spectroscopy of the reaction intermediates involved in the excited reaction.

IV. Results

A. Time-of-Flight Mass Spectra. Figure 3 shows time-of-flight mass spectra that result when a mixture of Ba vapor and CH_3F is coexpanded with helium as carrier gas and ionized at 266 nm. The fundamental output of the YAG laser (∼10 mJ/pulse) was used for vaporization to obtain the mass spectrum shown in the upper trace. When the infrared laser is used for desorption and accurate adjustments among the gas pulse, desorption, and excitation lasers are carried out, the Ba, BaOH, and BaF ion signals are minimized while the Ba···$(FCH_3)_n$, with $n = 1-3$, complexes are the majority. The lower trace shows the mass spectrum obtained when the second harmonic output of the same YAG (∼1 mJ/pulse) was used for vaporization.

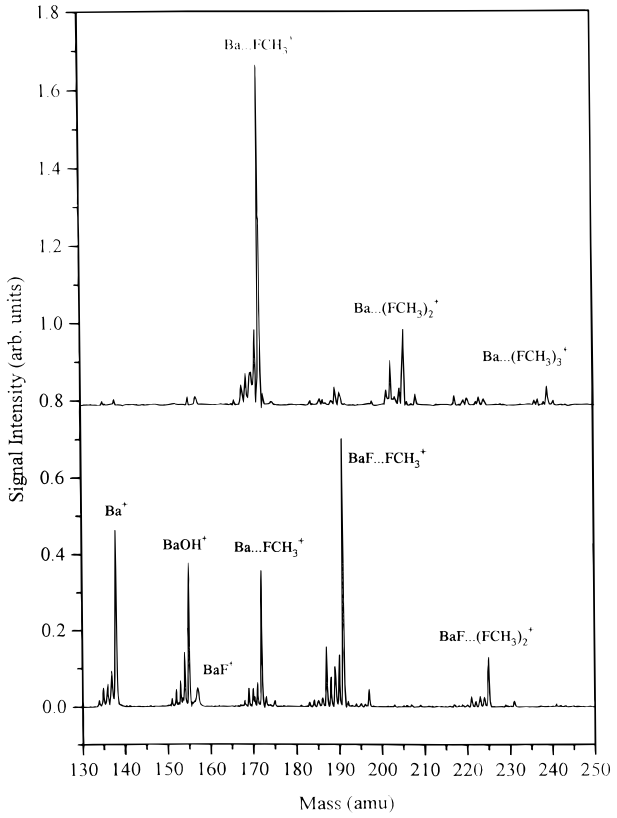

Figure 3. Time-of-flight mass spectra of the Ba + CH_3F system at 266 nm. Upper trace: TOFMS obtained using the fundamental output of the YAG laser for desorption. Lower trace: TOFMS obtained using the second harmonic output of the YAG for desorption.

The signal stability is higher with the second harmonic (∼15% maximum of fluctuation), but fine adjustments in the synchronization conditions do not allow to remove the Ba, BaOH, and BaF species from the ionization region. The barium hydroxide and oxide present in the molecular beam are oxidizing products of the metal. These oxide and hydroxide signals are stable with time, indicating that they are produced through the reaction of laser desorbed barium with water vapor present in the gas line. The production of metallic radicals in a supersonic environment through a chemical reaction has been reported. Whitham *et al.*[22] produced CaOH and other radicals through the reaction of the laser desorbed metal vapor with water and other gases. Pereira and Levy[23] reported the observation of CaOH and CaO as a result of the chemical reaction between water and laser desorbed calcium.

The most intense peaks appearing in the spectra correspond to species containing the ^{138}Ba isotope with the other four most abundant barium isotopes appearing at shorter flight times. In the lower trace, besides the masses already mentioned, the species BaF···FCH_3 can also be noticed.

The Ba, BaF, and Ba···FCH_3 ion signals were recorded as a function of the ionization laser energy at 266 nm; both Ba and BaF signals show clear two photon dependencies as can be expected from their ionization potentials of 5.21 and 4.8 eV, respectively. On the other hand, the Ba···FCH_3 signal shows a one photon dependence, providing an upper limit for its ionization potential, e.g., IP (Ba···FCH_3) ≤ 4.66 eV. The next section reports the experimental data which allowed a more accurate determination of this ionization potential.

B. Ba···FCH_3 Ionization Potential. In order to obtain a more accurate value of the ionization potential of the Ba··· FCH_3 complex, the signal intensity of the complex was monitored as the ionization wavelength was changed, keeping the laser power within the linear one photon regime. Figure 4

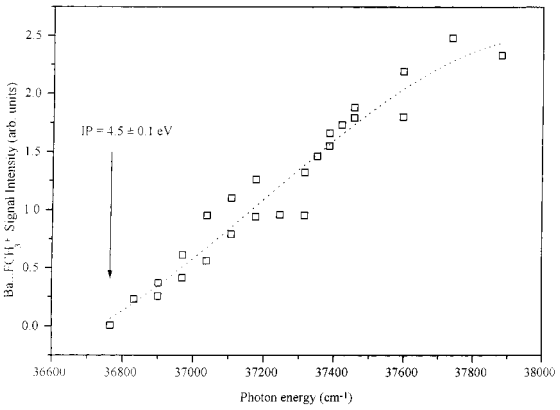

Figure 4. Ba···FCH_3 ion signal (open squares) as a function of the ionization laser energy. The displayed signal intensity is normalized at fixed laser energy fluence so that extrapolation to the energy threshold provides an estimate for the ionization potential of the complex, as indicated by the arrow. The dashed line was drawn through the points to help visualization.

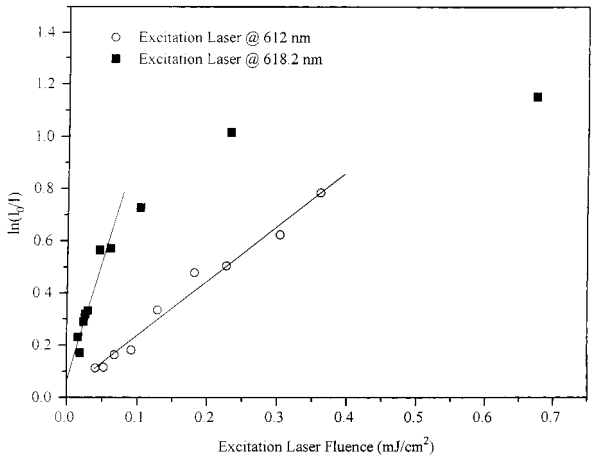

Figure 5. Laser energy fluence dependencies of the depletion signals of the Ba···FCH_3 complex at 618.2 and 612 nm, as indicated. The straight line is a fit to the data points. As can be seen, saturation starts at 0.1 mJ cm^{-2} for the 618.2 nm set of data.

presents this result, from which it is possible to deduce a value for the ionization potential of the Ba···FCH_3 complex of 4.5 ± 0.1 eV. It is seen that the ionization potential of the complex is lower than that of the free metal by 0.6 eV, indicating that the solvated Ba^+ is more stable than neutral Ba due to the presence of the solvent molecule. This result compares very well with that obtained by Polanyi *et al.*[15] for the Na···FCH_3 complex, whose ionization potential was found to be ca. 4.4 eV.

C. Photodepletion Spectrum. In order to obtain the photodepletion spectrum, the disappearance of the species was monitored as a function of the dye laser wavelength. For these processes the Beer−Lambert law can be written as[14,15]

$$\ln(N_0/N) = \sigma_d F \qquad (1)$$

in which N_0 (N) stands for the ion signal without (with) dye laser, F is the dye laser fluence, and σ_d the photodepletion cross-section as long as there is no saturation.[14,24−26] In order to meet this condition several scans, using different laser energies of the photodepletion laser, were carried out. The photodepletion cross-section was then calculated for each scan, and this process was repeated until a convergence limit for the cross-section value was reached. Figure 5 displays the laser fluence dependence of the depletion signal at 618.2 and 612 nm. The straight line in the diagram is obtained from a linear least-squares fit to the

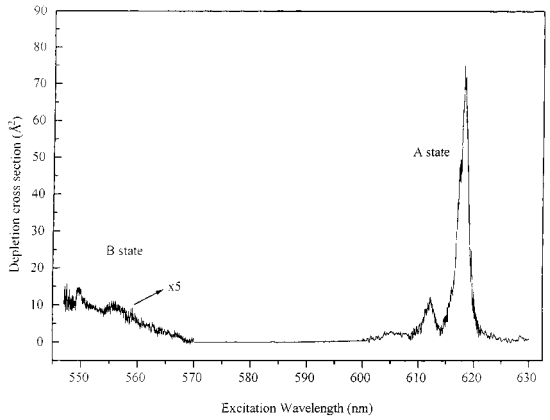

Figure 6. Photodepletion action spectrum of the Ba···FCH_3 complex in the 547−630 nm wavelength range. The second harmonic output was used for vaporization The two different regions assigned to distinct electronic states are clearly noticed.

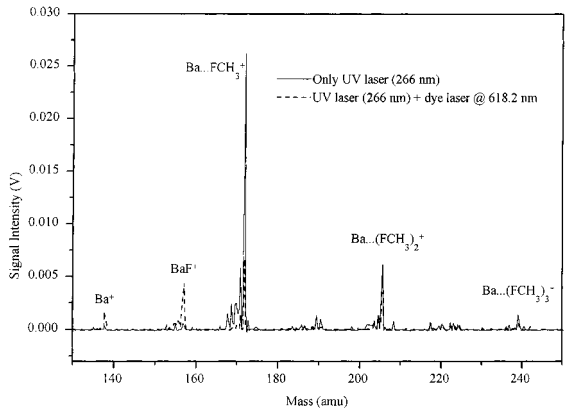

Figure 7. Photodepletion TOF mass spectrum at a fixed wavelength. The solid line shows the mass spectrum of the Ba···$(FCH_3)_n$ system when ionized by the fourth harmonic of the YAG laser. When the dye laser, tuned to 618.2 nm, interacts with the molecular beam, strong depletion from the Ba···FCH_3 complex is observed (dashed line). The enhancement of both Ba and BaF signals is clearly noticed as a result of complex photofragmentation.

data points with laser fluences lower than 0.08 mJ/cm^2 at 618.2 nm and 0.4 mJ/cm^2 at 612 nm. A linear relationship between $\ln(N_0/N)$ and F for Ba···FCH_3 is obtained for these fluences, while saturation effects are observed for higher fluences as clearly depicted at 618.2 nm.

Figure 6 shows the photodepletion spectrum of the ^{138}Ba··· FCH_3 complex in the range 547−630 nm. The metal was vaporized by the second harmonic output of the desorption laser (∼1 mJ/pulse). The spectrum is the result of averaging three different scans previously smoothed. Two well-differentiated regions can be noticed: one at longer wavelengths showing vibrational structure and high cross-sections (∼60−70 Å^2) and the other appearing at shorter wavelengths with significantly smaller cross-sections (∼1−4 Å^2) and a much more diffuse structure. The nature of these transitions will be discussed in terms of the spectroscopy and dynamics of this system in section V.

D. Photofragmentation Channels. Figure 7 shows a mass spectrum of the Ba···FCH_3 system. In this case, the vaporization of barium is produced with the fundamental output of the Nd:YAG laser (∼10 mJ/pulse) and the photodepletion is induced at 618.2 nm, which corresponds to the maximum observed in the photodepletion spectrum shown in Figure 6. The ionization laser is fixed at 266 nm. Strong depletion of the monomer is observed in the spectrum when the dye laser is allowed to enter into the chamber. However, no depletion is observed from the

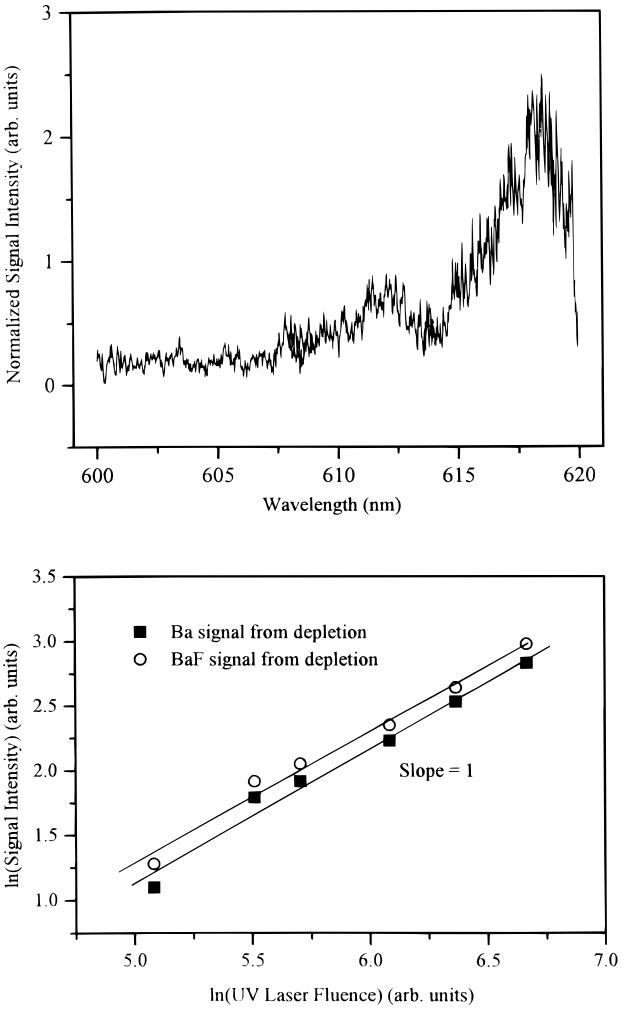

Figure 8. Top: Action spectrum of BaF in the range 600−620 nm. The BaF signal was monitored while the dye laser was scanned. Notice the close resemblance between this action spectrum and the total photodepletion spectrum depicted in Figure 6. Bottom: Laser energy fluence dependency of the Ba and BaF ion signals resulting from the Ba···FCH_3 complex fragmentation induced at 547 nm. Both signals show a single photon dependence, indicating that they emerge in excited states. See the energetic diagram displayed in Figure 2.

Ba···$(FCH_3)_n$ (n = 2, 3) species, indicating that these should probably absorb at different wavelengths. More work in this direction is underway.

A closer look at Figure 7 reveals an increase in intensity of the Ba and BaF species, suggesting two open channels for the complex fragmentation. The action spectrum for this reaction product can be obtained by monitoring the wavelength dependence of the BaF signal coming from the depletion of the complex. An example of it is presented in the upper part of Figure 8 over the 600−620 nm wavelength range. It is noticeable the close resemblance with the photodepletion spectrum. They actually appear as mirror images of each other. The Ba and BaF signals were recorded as a function of the ionization laser energy when the depletion was induced at 547 and 618.2 nm. They showed a clear single photon dependence with the UV laser (266 nm) when depleted at 547 nm, as is shown in the lower part of Figure 8. This single photon behavior indicates that these reaction products emerge in an excited state. Results when depleting at 618.2 nm show no such conclusive evidence for one photon dependence. This may be due to a major production of fragments in the ground state which makes it harder to analyze the results. Fluorescence experiments are in progress to study each of the photoreaction channels in detail and will be presented in a forthcoming publication.

V. Discussion

A. Structure of the Ba···FCH_3 Complex. The geometrical structure of the Ba···FCH_3 complex is an important factor in order to give a complete interpretation of the results presented in the preceding section. The possibility that the monomer structure would be BaF···CH_3 instead of Ba···FCH_3 can be ruled out if one considers the formation of excited Ba from monomer photodepletion with a photon of 618.2 nm (see Figure 2). Indeed the BaF···CH_3 structure can be excluded since the production of excited Ba as a photofragment is not energetically possible when such a BaF···CH_3 complex is excited with a 618.2 nm photon. In contrast, considering that the excitation energy associated with such a photon is of the order of 2.0 eV it becomes evident that only the excited Ba···FCH_3 complex can photofragment into metastable Ba.

There are no theoretical predictions about the geometry of this weakly bound complex. However, ab initio calculations suggest that the geometry of the Na···FCH_3 complex is bent.[15] Accordingly with a theoretical study by de Castro *et al.*,[18] the Ca···HX complexes studied by Soep's group[11−13] are all linear in the ground state. The Ca···HCl complex did show a vibrational progression with a spacing of ∼200 cm^{-1} that indicated a bent structure in the excited state.[12] The spacing of this progression is close to the progression found in this work for Ba···FCH_3 (ca. 150 cm^{-1}), which could also be consistent with a bent structure. However, there is not enough experimental evidence to exclude a linear geometry. Actually, the main conclusions derived from our results and their analysis do not depend on any specific assumption made on this matter.

B. Spectroscopy and Dynamics. *Resonances.* As is well-documented by Aquilanti and co-workers,[27,28] the effective potentials describing the interaction between an atom and a closed-shell molecule correlate adiabatically with the different spin−orbit states of the open-shell atom. As a result, this asymptotic region is fully characterized by the atomic total angular momentum j and its projection along the internuclear axis m_j. Accordingly we have only two different orientations of the excited p orbital of the barium atom with respect to the interaction axis, parallel and perpendicular. In the following we shall denominate these as A and B states, respectively. In this view, we have assigned the excited state involved in the transition at longer wavelengths (618.2 nm) to the A state of the complex, while the broad band appearing near the barium $^1S_0 \leftarrow {}^1P_1$ line (λ = 553.5 nm) is assigned to the B state. The much lower cross-section and lack of structure for the transition involving the upper excited state is basically attributed to spectroscopic factors (see Figure 10 below), e.g., to a shift of the excited potential energy surface with respect to the ground state surface leading to unfavorable Franck−Condon factors responsible for the very small depletion cross-section. This shift would imply a significant geometrical change of the complex in its B excited state with respect to that of the ground state. In contrast, the much higher depletion cross-section associated with the A excited state of the monomer, displaying also a well-defined vibrational structure, could reflect little geometrical change of the complex in its A state as compared to that of the ground state. This would favor the origin transition due to Franck−Condon factors for the subsequent depletion following laser excitation. We observed no features to the red of the 618.2 nm band, either in photodepletion or resonant-enhanced multiphoton ionization (REMPI) experiments, which supports our assignment of the 618.2 nm band as the band origin of this transition.

In Figure 8 of the previous section the action spectrum of the BaF species was shown. BaF appeared as the reaction product when the photodepletion laser was scanned over the

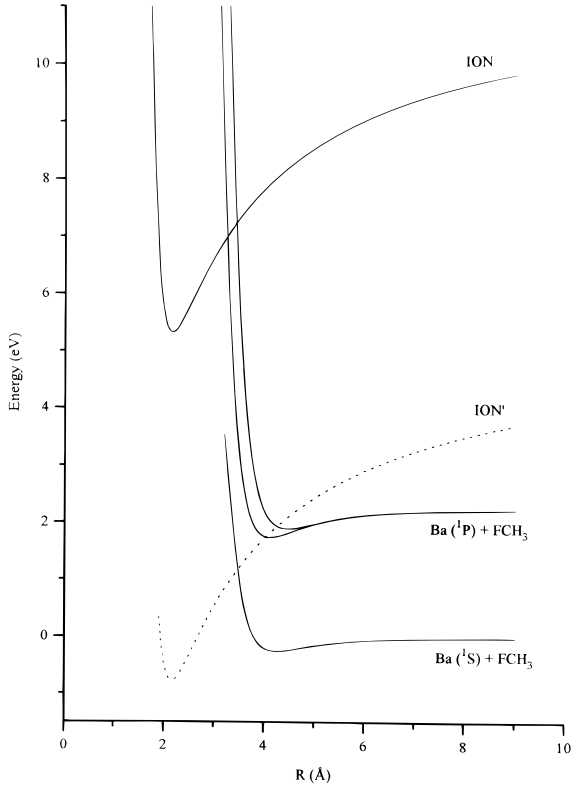

Figure 9. Approximate potential curves representing the Ba + CH_3F system. The curves for the ground and excited states of the complex were constructed using a 6−12 potential function. The curves of the ionic states were built using Born-type repulsion and Coulombic attraction. See Section V.B for a full description of the function and parameter values used.

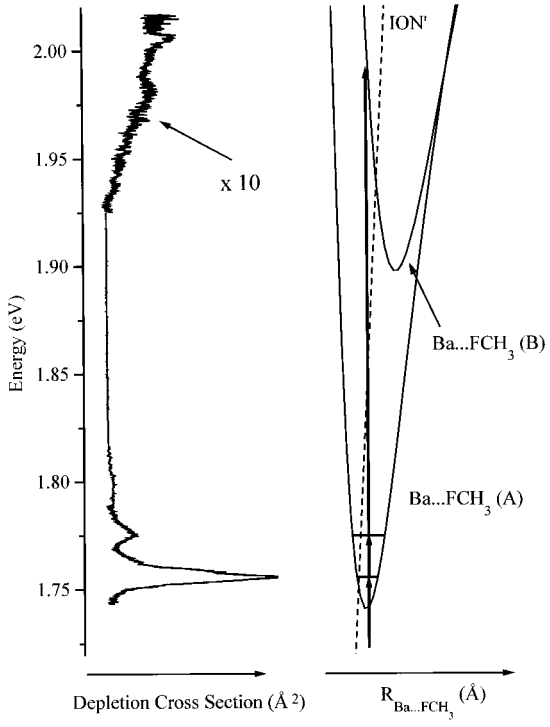

Figure 10. Simplified two-dimensional composition of the potential energy curves for the excited states of the Ba···FCH_3 complex (right) and the corresponding photodepletion spectrum (left). As indicated, the ordinate represents energy and the abscissa the Ba···FCH_3 interparticular distance. The combination uses the photodepletion spectrum of Figure 6 and the potential curves described in the text and shown in Figure 9.

600−620 nm range. This appearance is explained on the basis of an ionic−covalent curve crossing at the appropriate distance. In order to visualize this mechanism and the spectroscopic description mentioned above, we have built the approximate potential curves following Polanyi's scheme[15] with some modifications to take into account our experimental observations.

Figure 9 displays the approximate potential curves involved in these transitions, and Figure 10 gives a closer look showing the correlation between the observed photodepletion spectrum and the nature and crossing of the relevant potential energy curves involved in the spectroscopy and dynamics of the system. The potential curves of the weakly bound complex were calculated using a 6−12 potential function; $V(R) = A'/R^{12} - C_6/R^6$. The van der Waals coefficient, $C_6 = 3484$ eV Å^6, was calculated using the London formula with the ionization potentials of Ba and CH_3F being 5.2[29] and 12.8529[29] eV and the polarizabilities of Ba and CH_3F being 39.4[29] and 15.8[30] Å^3, respectively. The ionic interaction between Ba^+ and CH_3F^- is calculated using the Born-type repulsion and the Coulombic attraction, viz., $V(R) = (A'/R^{12}) - (e^2/R)$, the ionic bonding of Ba−F being 2.16 Å.[31] The asymptote of the ionic curve was obtained using the ionization potential of Ba and the electron affinity of CH_3F (−6.2 eV).[15]

It is seen in this diagram that the crossing of the covalent ground state and the first ionic state curves occurs at 2.9 Å, and at this distance a large energy barrier (6 eV) exists when the state goes from covalent to ionic. However, the relatively small photon energy at which the photodepletion occurs, producing BaF, was around 2.0 eV ($\lambda = 618.2$ nm), as can be seen in Figure 6. It is well-known from crossed-beam studies carried out with reactions proceeding through a harpooning mechanism[21] that the energy threshold corresponds to the minimum energy required to form the ionic negative potential of the reactant molecule, i.e., CH_3F in the present case. Since the well-accepted value of the electron affinity for this molecule—as mentioned above—is contradictory with the observed experimental threshold of 2.0 eV, one may suggest that not only the electronic excitation of the barium core facilitates the electron transfer but also a dramatic change in the C−F internuclear distance may be required for the reaction to occur. These molecules experience significant changes in their electron affinities as the halogen−carbon distance increases. In fact, the asymptotic value will be +3.45 eV, which is that of the F atom, e.g., at infinite C−F bond length. This argument has been previously considered by Polanyi's group in order to explain similar findings in the photodepletion spectra of Na···$(FCH_3)_n$. There are several studies both in gas phase and gas surface interactions which support this slackening effect in chemical bonds involved either in chemical reactions or charge transfer processes.[21,32,33] In this view the electron jump from the barium to the fluorine atom of the CH_3F molecule would be a result favored by the increase in the CH_3F electron affinity as well as by the reduction in the Ba ionization potential. Consequently, for the reaction to take place, the Ba···F distance would get shorter, while the C−F distance increases, so the ionic potential would reduce its energy producing ionic−covalent degeneracy that will finally favor the harpooning responsible for the reaction.

On the other hand Ayotte *et al.*[34] have studied absolute cross-sections for dissociative electron attachment (DEA) of methyl chloride and bromide physisorbed onto a Kr covered Pt substrate. They found DEA cross-sections several orders of magnitude higher than the corresponding gas phase values. Such enhancements in cross-sections were explained by a dramatic change in the survival probability of the methyl halide due to the lowering of its potential energy surface by polarization of the surrounding medium.

Obviously for the Ba···FCH_3 van der Waals molecule such a polarization effect cannot be expected to be as important as

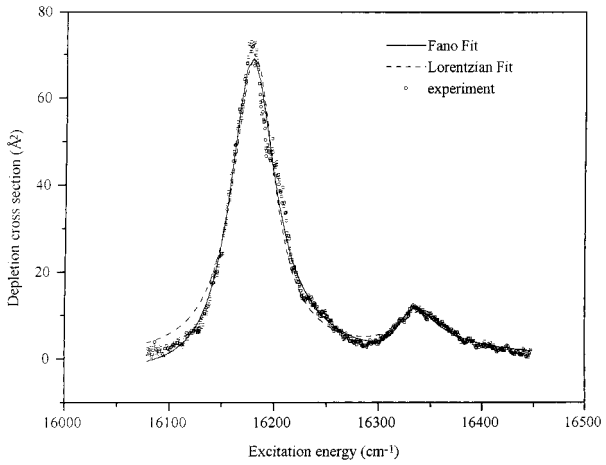

Figure 11. Fano and Lorentzian profiles fits of the bands appearing at 618.2 and 612 nm. The Fano function fits better than the Lorentzian one. See Section V.B for a discussion on their functionality and physical meaning.

TABLE 1. Best Fit Parameters of the Fano Function Obtained at the Indicated Spectral Bands (A State) for the A−X Transition of the Photodepletion Spectrum of the Ba···FCH_3 Complex

param	612 nm	std err	618.2 nm	std err
σ' (Å^2)	−2.98	0.21	−2.98	0.21
σ_0 (Å^2)	1.05	0.15	0.64	0.02
q	2.99	0.23	10.60	0.20
ν_0 (cm^{-1})	16 328.49	1.17	16 174.43	0.18
Γ (cm^{-1})	43.76	2.46	51.10	0.44

[a] See text and solid line of Figure 11.

if the CH_3F were physisorbed on a Ba surface; however, it should not be ruled out as a result of the significant Ba polarizability (see above). In this view, both effects, e.g., the C−F slackening and the CH_3F^- stabilization induced by the Ba polarization, may well contribute to initiation of the harpooning reaction at energies as low as 2.0 eV. It would be very interesting to determine the energy thresholds for van der Waals molecules containing several Ba atoms, e.g., for Ba_n···FCH_3 molecules with $n > 1$. This information would then provide more insight into the reaction mechanism and so critically assert the specific role of each effect.

A closer look at the band system that appears in the red part of the photodepletion spectrum shown in Figure 6 reveals that the bands appearing at 618.2 and 612 nm are asymmetric and reminiscent of Fano profiles,[35] in which sharp quasibound levels interfere with a broad continuum. These bands have been fitted to the Fano profile function:[36]

$$\sigma(\nu) = \sigma' + \sigma_0(q + \epsilon)^2/(1 + \epsilon^2) \qquad (2)$$

where

$$\epsilon = (\nu - \nu_0)/(\Gamma/2)$$

In this formula,[36] $\sigma(\nu)$ represents the total absorption cross-section, σ_0 is the background spectral cross-section, σ' is the cross-section for absorption into a noninteracting continuum, q is the asymmetry parameter, ν_0 is the center of the resonance, and Γ is the width of the resonance.

The result of these fits is displayed in Figure 11 together with a Lorentzian fit for comparison. The optimized parameters are given in Table 1. As can be seen in the figure, the experimental contours can be better fitted to a Fano than to a Lorentzian profile. The bandwidth of these peaks or resonances is related to the coupling of the quasibound levels with the

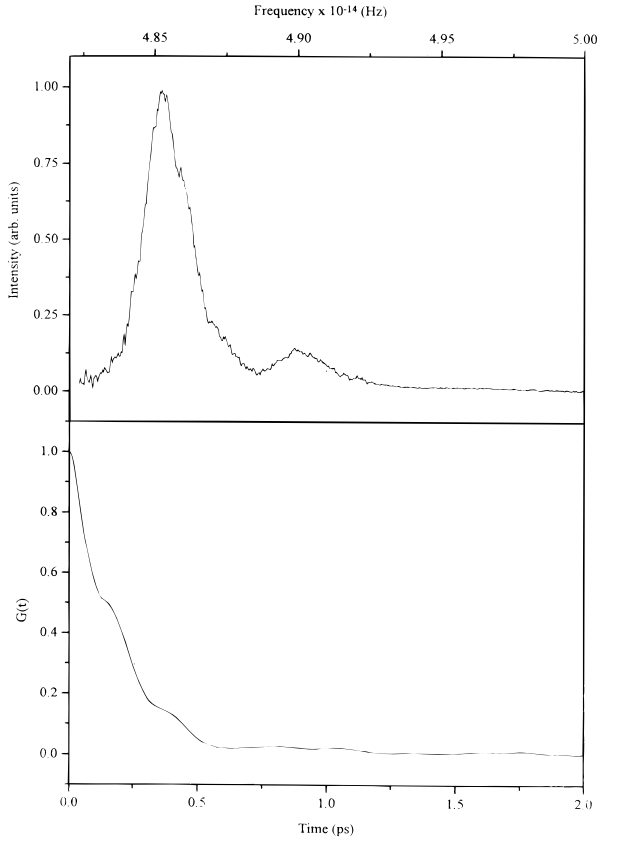

Figure 12. Top: photodepletion spectrum of the Ba···FCH_3 complex corresponding to the A−X transition. Bottom: Autocorrelation function, S(t), corresponding to the spectrum shown on top of the figure. This function has been normilized to 1 at $t = 0$.

continuum and, subsequently, with the lifetime of these excited states. Nevertheless, it is known that for these cases the full time behavior of the system can be obtained only by Fourier transformation of the entire spectrum.[37,38] This gives the so-called autocorrelation function, $S(t)$, which can be deduced directly from experiments by inverting the Fourier transform of the spectral band, $I(\omega)$, of interest, e.g.,

$$S(t) = \langle \mu(0)\, \mu(t) \rangle = \int d\omega \exp(i\omega t)\, I(\omega) \qquad (3)$$

in which μ is the transition dipole moment of the molecule and ω the angular frequency absorbed by it. The $S(t)$ function[38] contains the time evolution of the system in the excited potential. In Figure 12 the autocorrelation function corresponding to the longer wavelength region, the A state, is displayed. It becomes evident that the complex fragmentation significantly reduces its lifetime down to a few hundred femtoseconds (ca. 250 fs). In this view, the electron transfer process triggered by laser excitation is very fast, but there is still some coupling to the bound excited potential whose vibrational mode is of the order of 150 cm^{-1}, which corresponds to 220 fs. It is also clear how after a half-picosecond the excited state population is almost entirely depleted. It is also interesting to remark that this lifetime value is considerably shorter than the photodissociation time of a weakly bound complex, typically in the picosecond domain.[39] This would indicate that the factor controlling the bandwidth of the lines is the photoinduced reaction within the complex which gives BaF + CH_3, as well as some electronically excited Ba. In other words, it appears that the spectral features are basically controlled by the excited reaction dynamics, the harpooning process, rather than by the simple breaking of the van der Waals bond.

In spite of the above discussion about the excited complex lifetime, care must be taken in accepting the 250 fs value as a

proved result. It is well-known that for polyatomic molecules lifetimes deduced from absorption spectra may differ from those measured through femtosecond experiments, as evidenced by Mestdagh *et al.*[40] In consequence this value should be considered as a preliminary estimation until direct femtosecond experiments carried out on this system allow it to be confirmed.

VI. Concluding Remarks

The experimental setup implemented in our laboratory to investigate the spectroscopy and dynamics of weakly bound complexes has been described. The complexes were formed in supersonic expansions of laser vaporized metals and detected by laser ionization time-of-flight mass spectrometry. While the mass resolution allows a clear identification of the excited complex as well as of any fragment, the spectroscopic analysis, typically under the usual pump and probe configuration, provides information on the internal structure of the reaction intermediate. The results reported correspond to laser ionization and photodepletion spectra of the $Ba\cdots(FCH_3)_n$ for $1 \leq n \leq 3$ weakly bound complex. Basically, the present work has been dedicated to the study of the monomer whose ionization potential was found to be IP $= 4.5 \pm 0.1$ eV.

One of the main results of the present study was the photodepletion action spectrum of the $Ba\cdots FCH_3$ complex. It contained two well-defined and distinct regions which were assigned to two different electronic states: A and B states. At longer wavelengths it showed a high cross-section ($60-70$ Å^2) and a well-defined vibrational structure, while a much smaller cross-section ($2-4$ Å^2), with a more diffuse structure, appeared at shorter wavelengths. In addition, clear resonances were observed at longer wavelengths which were rationalized by involving a significant coupling between the bound excited potential of the complex and the (open channel) ionic potential leading to $BaF^* + CH_3$ reaction products. The autocorrelation function corresponding to the longer wavelength region, the A state, suggested that the fragmentation of the complex significantly reduces its lifetime down to a few hundred femtoseconds (ca. 250 fs). A reaction picture was drawn which consisted of visualizing the electron transfer process, triggered by laser excitation, as a very fast process but with still some coupling to the bound vibrational mode of the excited potential. It was also pointed out how after a half-picosecond the excited state population is almost entirely depleted. Of course real time experiments carried out with femtosecond lasers are suggested and will be neccessary to confirm our suggested value of 250 fs for the excited complex lifetime.

Preliminary results on the complex photofragmentation indicated that both Ba and BaF are produced. Whereas fragmentation from the excited B state clearly produced electronically excited Ba and BaF, no such clear evidence can be drawn for the A state. This was attributed to a significant yield of Ba and BaF in their ground states. To confirm this point, a full analysis of the different photofragmentation channels is now in progress in our laboratory for which laser induced fluorescence experiments are also planned and will be the subject of a forthcoming publication.

Acknowledgment. S.S. acknowledges a predoctoral fellowship under Contract CT92-0011 of the EEC Human Capital and Mobility Programme. R.P. thanks the DGICYT of the Ministry of Education and Culture of Spain for a postdoctoral contract. This work has received financial support from the DGICYT of Spain (Grants PB91/357 and PB95/391).

References and Notes

(1) Levine, R. D.; Bernstein, R. B. *Molecular Reaction Dynamics and Chemical Reactivity*; Oxford University Press: Oxford, U.K., 1987.
(2) Brooks, P. R. *Chem. Rev.* **1988**, *88*, 407.
(3) Zewail, A. H. *Science* **1988**, *242*, 1645.
(4) Zewail, A. H. *Faraday Discuss. Chem. Soc*. **1991**, *91*, 207.
(5) Polanyi, J. C.; Zewail, A. H. *Acc. Chem. Res*. **1995**, *28*, 119.
(6) Garay, M.; González Ureña, A. Manuscript in preparation.
(7) Jouvet, C.; Boiveneau, M.; Duval M. C.; Soep, B. *J. Phys. Chem.* **1987**, *91*, 5416.
(8) Wittig, C.; Sharpe, S.; Beaudet, R. A. *Acc. Chem. Res.* **1988**, *21*, 341.
(9) Weaver, A.; Metz, R. B.; Bradforth, S. E.; Newmark, D. M. *J. Phys. Chem*. **1988**, *92*, 5558.
(10) Jouvet, C.; Soep, B. *Laser Chem*. **1985**, *5*, 157.
(11) Soep, B.; Abbes, S.; Keller, A.; Visticot, J. P. *J. Chem. Phys*. **1992**, *96*, 440.
(12) Soep, B.; Whitham, C. J.; Keller, A.; Visticot, J. P. *Farady Discuss. Chem. Soc*. **1991**, *91*, 191.
(13) Keller, A.; Lawruszczuk, R.; Soep B.; Visticot, J. P. *J. Chem. Phys*. **1996**, *105*, 4556.
(14) Liu, K.; Polanyi, J. C.; Yang, S. *J. Chem. Phys*. **1993**, *98*, 5431.
(15) Polanyi, J. C.; Wang, J.-X. *J. Phys. Chem*. **1995**, *99*, 13691.
(16) Hopkins, J. B.; Langridge-Smith, P. R. R.; Morse, M. D.; Smalley, R. E. *J. Chem. Phys*. **1983**, *78*, 1627.
(17) Cable, J. R.; Tubergen, M. J.; Levy, D. H. *J. Am. Chem. Soc*. **1988**, *110*, 7349.
(18) de Castro, M.; Candori, R.; Pirani, F.; Aquilanti, V.; Garay, M.; González Ureña, A. *Chem. Phys. Lett.* **1996**, *263*, 456.
(19) Smith, G. P.; Whitehead, J. C.; Zare, R. N. *J. Chem. Phys.* **1977**, *67*, 4912.
(20) Wu, K. T. *J. Phys. Chem*. **1979**, *83*, 1043.
(21) González Ureña, A. *Adv. Chem. Phys*. **1987**, *66*, 213.
(22) Whitham, C. J.; Soep, B.; Visticot, J. P.; Keller, A. *J. Chem. Phys*. **1990**, *93*, 991.
(23) Pereira, R.; Levy, D. H. *J. Chem. Phys*. **1996**, *105*, 9733.
(24) Buck, U. In *Dynamics of Polyatomics van der Waals Complexes*; NATO Advanced Study Institute, Series B: Physics; Halberstadt, N., Janda, K. C., Eds.; Plenum: New York, 1990; Vol. 227.
(25) Wang, C. R.; Pollack, S.; Cameron, D.; Kappes, M. M. *J. Chem. Phys*. **1990**, *93*, 3787.
(26) Selby, K.; Kresin, V.; Masui, J.; Vollmer, M.; Scheidemann, A.; Knight, W. D. *Z. Phys: D* **1991**, *19*, 43.
(27) Aquilanti, V.; Liuti, G.; Pirani, F.; Vecchiocativi, F. *J. Chem. Soc., Faraday Trans. 2* **1989**, *85*, 955.
(28) de Castro Vitores, M.; Candori, R.; Pirani, F.; Aquilanti, V.; Menéndez, M.; Garay, M.; González Ureña, A. *J. Phys. Chem*. **1996**, *100*, 7997.
(29) *CRC Handbook of Chemistry and Physics*, 74th ed.; Lide, D. R., Ed.; CRC Press: Boca Raton, FL, 1993.
(30) Rice, J. E.; Amos, R. D.; Colwell, S. M.; Handy, N. C.; Sanz, J. *J. Chem. Phys.* **1990**, *93*, 8828.
(31) Huber, K. P.; Herzberg, G. *Molecular Spectra and Molecular Structure IV. Constants of Diatomic Molecules*; Van Nostrand: Reinhold: New York, 1979.
(32) Castaño, J.; Zapata, V.; Makarov, G.; González Ureña, A. *J. Phys. Chem.* **1995**, *99*, 13659.
(33) Kleyn, A. W.; Los, J. E.; Gislason, A. *Phys. Rep*. **1982**, *91*, 1.
(34) Ayotte, P.; Gamache, J.; Bass, A. D.; Fabrikant, I. I.; Sanche, L. *J. Chem. Phys*. **1997**, *106*, 749.
(35) Fano, U. *Phys. Rev*. **1961**, *124*, 1866.
(36) Brandon, J. T.; Reild, S. A.; Robie, D. C.; Reisler, H. *J. Chem. Phys.* **1992**, *97*, 5246.
(37) Heller, E. J. *Acc. Chem. Res*. **1981**, *14*, 368.
(38) Schinke, R. *Photodissociation Dynamics*; Cambridge University Press: Cambridge, U.K., 1992.
(39) Krim, L.; Soep, B.; Visticot, J. P. *J. Chem. Phys*. **1995**, *103*, 9589.
(40) Mestdagh, J. M.; Berdah, M.; Dimicoli, I.; Mons, M.; Meynadier, P.; d'Oliveira, P.; Piuzzi, F.; Visticot, J. P.; Jouvet, C.; Lardeux-Dedonder, C.; Martrenchard-Barra, S.; Soep, B.; Solgadi, D. *J. Chem. Phys*. **1995**, *103*, 1013.